Optimal Capacity Configuration of Large-scale Energy Bases Considering External Multi-stochastic Scenarios and Interactive Multi-timescale Objectives

Yini Wang, Yang Hu, Yueli Zhao, Yunzhi Li, Fang Fang, and Jizhen Liu

***Abstract*—Optimal capacity configuration (OCC) of large-scale energy bases with multi-timescale operation characteristics presents a critical challenge. To address the problem, this study proposes an OCC approach of large-scale energy bases considering external multi-stochastic scenarios and interactive multi-timescale objectives. Firstly, guided by the system theory, the nonlinear state-space description is presented for systematic analysis of a general large-scale energy base. Due to interactive multi-timescale objectives between annual and daily cumulative objectives, a nested optimization structure is established. Then, considering the external multi-stochastic scenarios caused by the variables such as wind speed, solar irradiance, electric load, and thermal load, a multi-step optimization strategy is proposed including pre-configuration in regular scenarios and re-configuration by introducing micro-incremental scenarios. The multi-step optimization strategy and nested optimization structure jointly achieve the OCC of the large-scale energy base. In each step, the nested optimization structure is executed once. Finally, while ensuring the balance between thermal supply and load demand, the imbalances between electric power supply and the load demand are eliminated, significantly showing the efficiency of the proposed OCC approach.**

***Index Terms*—Large-scale energy base, optimal capacity configuration, multi-timescale objective, nested optimization, multi-stochastic scenario.**

I. Introduction

With the increasing depletion of fossil energy sources, the global community is confronting an imminent energy crisis [1]. Ongoing advancement of renewable energy technologies is expected to significantly accelerate the worldwide transition to low-carbon energy systems. However, due to the dual stochasticity from both the renewable energy power generation and demand, how to achieve the optimal capacities for electric power, thermal power, or storage units becomes a critical challenge.

For integrated energy systems (IESs), the optimal capacity configuration (OCC) procedure includes the definition of optimization objectives, the determination of constraints, and the optimization problem solving. Besides, there are single-objective optimization [2]-[6] with economic costs throughout the whole life cycle and net present value, and multi-objective optimization [7]-[10] with metrics such as investment cost, carbon emission, and energy supply reliability. Operation data or characteristic models of various units are often used as constraints. Finding the OCC is a fundamental optimization problem, and is often approached using algorithms such as cycle traversal [11], game theory [12], convex optimization [13], and heuristic intelligent optimization [14]-[16].

To address the dual stochasticity, scenario analysis approaches are used for OCC of IESs. In [17], multiple scenarios and their probabilities are obtained through scenario generation and reduction based on the joint probability density function of electric load, wind power, and photovoltaic (PV) power, transforming the problem into multiple deterministic problems. The Latin hypercube sampling is used to simulate scenarios with three stochastic variables, i.e., wind speed, solar irradiance, and electric power load, and 27 typical scenarios from the spring, winter, and transition seasons are preserved [18]. The joint uncertainties of source and load are not considered. Copula functions could construct joint probability distribution for variables with different probability distributions [19], which are useful to generate multi-stochastic scenarios.

In order to better describe the correlation of stochastic variables on source and load sides, deep generation algorithms are used for scenario generation. Reference [20] generates wind speed scenarios by ensemble neural network for OCC of energy storage. Based on two-stage stochastic planning [21], artificial neural networks are used for scenario

Manuscript received: August 5, 2024; revised: January 14, 2025; accepted: April 19, 2025. Date of CrossCheck: April 19, 2025. Date of online publication: May 2, 2025.

This work was supported by the National Key R&D Program of China (No. 2021YFE0102400) and the National Natural Science Foundation of China (No. 51906064).

Y. Wang, Y. Hu (corresponding author), F. Fang, and J. Liu are with the State Key Laboratory of Alternate Electrical Power System with Renewable Energy Sources (North China Electric Power University), Beijing 102206, China, and they are also with the School of Control and Computer Engineering, North China Electric Power University, Beijing 102206, China (e-mail: wangyini@ncepu.edu.cn; hooyoung@ncepu.edu.cn; fangfang@ncepu.edu.cn; ljz@ncepu.edu.cn).

Y. Zhao and Y. Li are with the School of Control and Computer Engineering, North China Electric Power University, Beijing 102206, China (e-mail: yuelizhao5@gmail.com; liyzhi@ncepu.edu.cn).

DOI: 10.35833/MPCE.2024.000869

generation of solar irradiance. Based on federated deep generative learning, scenario generation of wind and PV power is presented in [22]. Conditional deep convolutional generative adversarial network (CDC-GAN) could generate scenarios containing temporal and spatial implicit correlations. To ensure that the generated scenarios have the same probability distribution as the original ones, Wasserstein distance [23] is introduced to CDC-GAN. Reference [24] utilizes an improved algorithm to generate scenarios for different seasons. However, in these studies, it is not possible to get each potential scenario.

Different from traditional small IESs, large-scale energy bases face more complex spatio-temporal scales and stronger uncertainties from source and load sides. OCC of large-scale energy bases for various units needs to be compatible with more stochastic scenarios. Reference [25] investigates the planning of fast frequency response reserves in power systems under homogeneous extreme risks. In contrast, [26] proposes a metric for assessing the resilience value, which could accurately quantify the resilient support role played by energy storage systems during extreme events. Both studies are dedicated to addressing the challenges confronted by the power systems under unconventional circumstances.

To enhance the feasibility of OCC results, [27] uses the box uncertainty set to generate typical wind speed scenarios and presents a bi-level structure to plan an integrated system with electric power and natural gas. In [28], Monte Carlo simulation is adopted to generate stochastic scenarios and solve two-stage mixed-integer linear programming. However, most studies only consider the economic cost and neglect other attributes for optimization.

The widespread integration of a high proportion of renewable energy has greatly changed the operation and control of power systems. How to deal with uncertainties on the source and load sides and make the OCC of units more economical, effective, and reliable becomes the critical problems that need to be addressed.

By introducing system theory, we abstract a large-scale energy base into a multi-input and multi-output system, which considers the impact of internal and external factors and proposes an OCC approach of large-scale energy bases. The main contributions of this study are as follows.

1) System theory is introduced to represent a large-scale energy base by a multi-input and multi-output nonlinear state-space description, which assists the systematic analysis of external multi-stochastic scenarios and interactive multi-timescale objectives during OCC process.

2) Due to the interactive multi-timescale objectives between annual and daily cumulative objectives, a nested optimization structure is established including upper- and lower-level optimization using annual and daily cumulative objectives. A multi-dimensional optimization space with economy (investment cost), output fluctuation (mean variance fluctuation of load), and carbon emission is constructed while improving the solving efficiency via hierarchical structure.

3) By fully considering the external multi-stochastic scenarios, a multi-step optimization strategy is proposed including pre-configuration with regular scenarios and re-configuration by introducing micro-incremental scenarios. The imbalances between power supply and load demand are eliminated.

The rest of the study is organized as follows. Section II provides systematic descriptions and analysis. Section III proposes the multi-step optimization strategy with nested optimization structure. Section IV elucidates the generation of regular scenarios as well as pre-configuration. Section V discusses re-configuration by introducing micro-incremental scenarios. Section VI shows the validation and analysis. Section VII summarizes the completed work.

II. Systematic Descriptions and Analysis

A. Architecture of a General Large-scale Energy Base

According to the China's 14th Five Year Plan, the large-scale energy bases can supply both thermal and electric power. The planning of large-scale energy base necessitates a consideration of not only the characteristics of thermal or power load but also the inherent traits of renewable energy sources, including wind velocity and solar radiation intensity.

This study examines three categories of energy demand: electric power, thermal power, and hydrogen. The energy base consists of PV power units, wind power units, pure thermal power units, combined thermal and power (CHP) units, hydrogen fuel cells, vanadium redox flow batteries (VRBs), and hydrogen and thermal storage units.

When wind power and PV power account for a very high proportion, stronger fluctuations would create the imbalance between supply and demand, which may trigger localized load losses or wind/PV power curtailment during specific operation periods. Due to that the electric and thermal power consumption on the load side is also stochastic, conventional power sources and energy storage systems are essential to balance power supply deficit and store excess electricity.

The thermal power units serve as critical backup capacity, ensuring stable power supply to the large-scale energy base by interfacing with the power grid. This integration enhances grid reliability, especially during periods of renewable energy intermittency or load fluctuations. CHP units further optimize energy efficiency by simultaneously producing electric and thermal power, leveraging waste thermal recovery to meet both electric and thermal power demands. Electro-thermal converters facilitate the transformation of excess electric power into thermal power, enabling seasonal or on-demand thermal power supply. The energy storage unit comprises electro-chemical storage for electric power buffering and thermal power storage units for thermal retention, collectively ensuring system flexibility and resilience against supply and demand imbalance.

The hydrogen energy system consists of an electrolyzer that converts electric power into green hydrogen, a storage facility for compressed hydrogen, and a fuel cell that converts the green hydrogen into electric power. The combination of hydrogen storage unit and hydrogen consumption unit will increase the potential for flexible dispatch of hydro-

gen energy, improve energy utilization efficiency, and share the supply pressure during periods of high load demand.

B. Systematic Analysis from a Perspective of System Theory

Large-scale energy bases are distributed across vast geographical areas, with numerous physical devices and complex interconnections. From the perspective of system theory, large-scale energy base is viewed as a complex system whose characteristics can be briefly described by the following nonlinear state-space equation:

$$\begin{cases} \dot{\boldsymbol{x}} = f(\boldsymbol{x}, \boldsymbol{u}, \boldsymbol{v}) \\ \boldsymbol{y} = g(\boldsymbol{x}, \boldsymbol{u}, \boldsymbol{v}) \end{cases} \tag{1}$$

where $\boldsymbol{x}$ is the vector representing the internal states; $\boldsymbol{y}$ is the vector representing the system outputs; $\boldsymbol{u}$ is the vector representing system control inputs; $\boldsymbol{v}$ is the vector representing the external stochastic disturbances; and $f(\cdot)$ and $g(\cdot)$ are the nonlinear functions.

External stochastic factors are the main challenges for the OCC of various units because the external scenarios composed of several stochastic variables are constantly changing. This renders the consideration of external multi-stochastic scenarios as a core element in the OCC process of large-scale energy bases. Thus, the OCC problem should fully consider multi-stochastic scenarios.

According to the architecture of a general large-scale energy base, the relationships among variables are shown in Supplementary Material A Fig. SA1 from system theory. The operation dynamics of different units and system-level operation dynamics exist at different timescales. Therefore, when the OCC is performed, it is necessary to consider the issues of collaborative interaction between multi-timescale objectives of different units and the system level. Then, the OCC problem should define interactive multi-timescale objectives.

On this basis, a nested optimization structure is proposed including the upper-level optimization with annual cumulative objectives and the lower-level optimization with daily cumulative objectives. It could decompose a huge optimization problem into two levels, improving the efficiency and quality of optimization solutions.

Furthermore, the stochastic variables such as wind speed, solar irradiance, electric power load, and thermal power load are used to define the stochastic scenario vector. For the external multi-stochastic scenarios with different probabilities, a multi-step optimization strategy is presented including the pre-configuration in the regular scenarios and the re-configuration in the micro-incremental scenarios.

III. Multi-step Optimization Strategy with Nested Optimization Structure

A. Interactive Multi-timescale Objectives in Nested Optimization Structure

A nested optimization structure is constructed to coordinate the capacity planning of each unit within a large-scale energy base to achieve the optimization performance of multi-timescale objective.

The upper-level optimization determines the rated capacity of each energy supply source, which is regarded as the input of the lower-level optimization. The lower-level optimization is to determine the optimal operation revenue of the energy base for each typical day while ensuring the safety and reliability of energy supply. The resulting outputs are fed back to the upper-level optimization to determine the final capacities.

1) Upper-level Optimization by Annual Cumulative Objectives

The objective function for upper-level optimization is:

$$\min F_{Upper} = \{F_1, F_2, F_3\} \tag{2}$$

where F_1, F_2, and F_3 denote the economy, output fluctuation, and carbon emission of a large-scale energy base, respectively.

1) The economy of a large-scale energy base is evaluated by:

$$\min F_1 = \sum_{i \in \Omega} c_{i,con} P_{i,rated} f_{i,cr} + 365 F^*_{lower} \tag{3}$$

$$f_{i,cr} = \frac{r(1+r)^{L_i}}{(1+r)^{L_i} - 1} \tag{4}$$

where Ω is a set containing power generation units, thermal generation units, hydrogen production units, thermal storage units, power storage units, and hydrogen storage units; $c_{i,con}$ is the capacity cost of unit i; $P_{i,rated}$ is the rated capacity of unit i; $f_{i,cr}$ is the depreciation cost of unit i; r is the discount rate; L_i is the service life of unit i; and F^*_{lower} is the optimal objective value obtained from the lower-level optimization.

2) The output fluctuation is evaluated by:

$$\min F_2 = \sum_{s \in S} \sum_{t=1}^{T} \left(P(t,s) - P_{ave}(t,s) \right)^2 \Big/ T \tag{5}$$

$$P(t,s) = \sum_{i \in \Omega} P_i(t,s) \tag{6}$$

$$P_{ave}(t,s) = \sum_{t=1}^{T} \left(\sum_{i \in \Omega} P_i(t,s) \right) \Big/ T \tag{7}$$

where T is the time period; S is the set covering all the selected scenarios, with s being one of the scenarios; $P_i(t,s)$ is the output of unit i during time period t in scenario s, which is obtained from the lower-level optimization; and $P_{ave}(t,s)$ is the mean output of units during time period t in scenario s.

The integration of hydrogen energy enables the satisfaction of load demands while avoiding carbon emissions, enhancing energy efficiency and advancing environmental sustainability. Consequently, the primary carbon emissions stem not solely from pure thermal and CHP units, but also arise from interactions between the energy base and power grid [29].

3) The carbon emission is evaluated by:

$$\min F_3 = \sum_{s \in S} \sum_{t=1}^{T} \left[\mu \left(P_{grid}(t,s) + P_{TP}(t,s) \right) + \gamma P_{CHP}(t,s) \right] \tag{8}$$

where μ and γ are the carbon emission coefficients of pure thermal power and CHP units, respectively; and P_{grid}, P_{TP}, and P_{CHP} are the outputs of power grid, pure thermal power

units, and CHP units, respectively.

Upper-level capacity planning is subject to the capacity constraints and is optimized within the operation capacity of the large-scale energy base, while ensuring the compatibility with individual device specifications.

2) Lower-level Optimization by Daily Cumulative Objectives

This part formulates the objective function and constraints of the lower-level optimization. It is worth noting that the objective function is calculated using a daily cumulative manner, which involves summing the data for each hour throughout the day.

$$\min F_{lower} = \sum_{i\in\Omega}\sum_{t=1}^{T}\left(\sum_{s\in S}\pi_s c_{i,ope}P_i(t,s)\right) \tag{9}$$

where π_s is the probability of scenario s; and $c_{i,ope}$ is the operation cost coefficient of unit i, calculated at one percent of the investment cost coefficient.

In the large-scale energy base, the constraints of the lower-level optimization consist of load balance, power limitation, and capacity limitation. The optimization space is defined by both equality and inequality constraints.

1) In every scenario, the load balance constraints should be satisfied at all time instants:

$$H_{CHP}(t,s)+H_{EB}(t,s)+H_{HST}(t,s)-H_L(t,s)=0 \tag{10}$$

$$P_{PV}(t,s)+P_{WT}(t,s)+P_{grid}(t,s)+P_{CHP}(t,s)+P_{TP}(t,s)+P_{HCSS}(t,s)+P_{VRB}(t,s)-P_{EB}(t,s)-P_L(t,s)=0 \tag{11}$$

where P_{PV} and P_{WT} are the outputs of PV power and wind power, respectively; P_{HCSS} is the output power of the hydrogen fuel cell minus the power consumption of the hydrogen electrolysis unit; P_{VRB} is the output of VRBs; P_{EB} is the power consumption of electric-heating molten salt boiler; P_L is the electric power demand; H_{CHP}, H_{EB}, and H_{HST} are the thermal power outputs of CHP unit, electric-heating molten salt boiler, and thermal storage unit, respectively; and H_L is the thermal demand.

2) The power limitation constraints are:

$$P_i^{\min}\le P_i(t,s)\le P_i^{\max} \tag{12}$$

where $P_i^{\min}$ and $P_i^{\max}$ are the minimum and maximum outputs of unit i, respectively. The upper and lower limits of each unit are calculated based on the unit rated capacity provided by the upper-level optimization.

3) The charging and discharging states of energy storage units are introduced. For various energy types, the capacity limitation constraints can be expressed as:

$$S_*(t,s)=(1-\sigma)S_*(t-\Delta t,s)+\lambda_c P^c(t,s)\Delta t-\frac{P^d(t,s)\Delta t}{\lambda_d} \tag{13}$$

$$SOC_*(t,s)=\frac{S_*(t,s)}{S_*^r} \tag{14}$$

where S_* is the current state of unit * and the symbol * denotes battery storage units or thermal storage units; σ, λ_c, and λ_d are the self-discharging rate, storage efficiency, and release efficiency of storage units, respectively; S_*^r is the rated capacity of unit *, provided by the upper-level optimization; SOC_* is the state of charge of unit *; and P^c and P^d are the charging and discharging power, respectively.

Equations (15)-(17) ensure that the remaining energies of VRBs S_{VRB}, hydrogen storage unit S_{H_2}, and thermal storage unit S_{HST} vary within the specified interval.

$$S_{VRB}^{\min}\le S_{VRB}(t,s)\le S_{VRB}^{\max} \tag{15}$$

$$S_{HST}^{\min}\le S_{HST}(t,s)\le S_{HST}^{\max} \tag{16}$$

$$S_{H_2}^{\min}\le S_{H_2}(t,s)\le S_{H_2}^{\max} \tag{17}$$

where the superscripts min and max denote the upper and lower energy storage limits of the unit, respectively, which are calculated based on S_*^r.

Capacity constraints of grid tie lines are:

$$-P_{grid}^{\max}\le P_{grid}(t,s)\le P_{grid}^{\max} \tag{18}$$

where $P_{grid}^{\max}$ is the maximum power of bidirectional transmission between the power grid and the large-scale energy base.

B. Multi-step Optimization in External Multi-stochastic Scenarios

This study develops a multi-step optimization strategy to achieve efficient operation of a large-scale energy base under varying external conditions. This strategy, visually outlined in Fig. 1, comprises two distinct steps: pre-configuration and re-configuration, each leveraging a bi-level nested optimization structure tailored to achieve its optimal results. In Fig. 1, S' is the set of micro-incremental scenarios.

The pre-configuration step is carried out based on annual and daily cumulative operation metrics. These metrics form the foundation for determining and evaluating the OCC effect, ensuring the advantages of the configuration scheme in both long-term and daily operations. To capture the inherent uncertainties, this step utilizes CDC-GAN to complete scenario generation and then reduces these scenarios using the simultaneous backward algorithm to obtain a regular set of scenarios. In this step, the optimized capacities of the units in the energy base are determined by the nested optimization structure within the regular scenario set.

The upper-level optimization is performed using the non-dominated sorting genetic algorithm III (NSGA-III). The algorithm is initialized with a set of parameters and then iteratively optimizes the upper-level decisions. The algorithm forms a new parent population, retains individuals based on fast non-dominated sorting and association with reference points, and performs fast non-dominated sorting to guide the search for Pareto-optimal solutions [30]. Decisions at this level depend on the daily operation and its associated benefits communicated from the lower-level optimization.

The lower-level optimization concentrates on daily operation, ensuring the execution of the upper-level plans while considering various practical constraints. The goal of this level is to determine the best daily scheduling plan, which is based on the capacities of various units provided by the upper level. In contrast, the re-configuration step refines the results of the pre-configuration to enhance the robustness. The re-configuration step is triggered by the identification of micro-incremental scenarios.

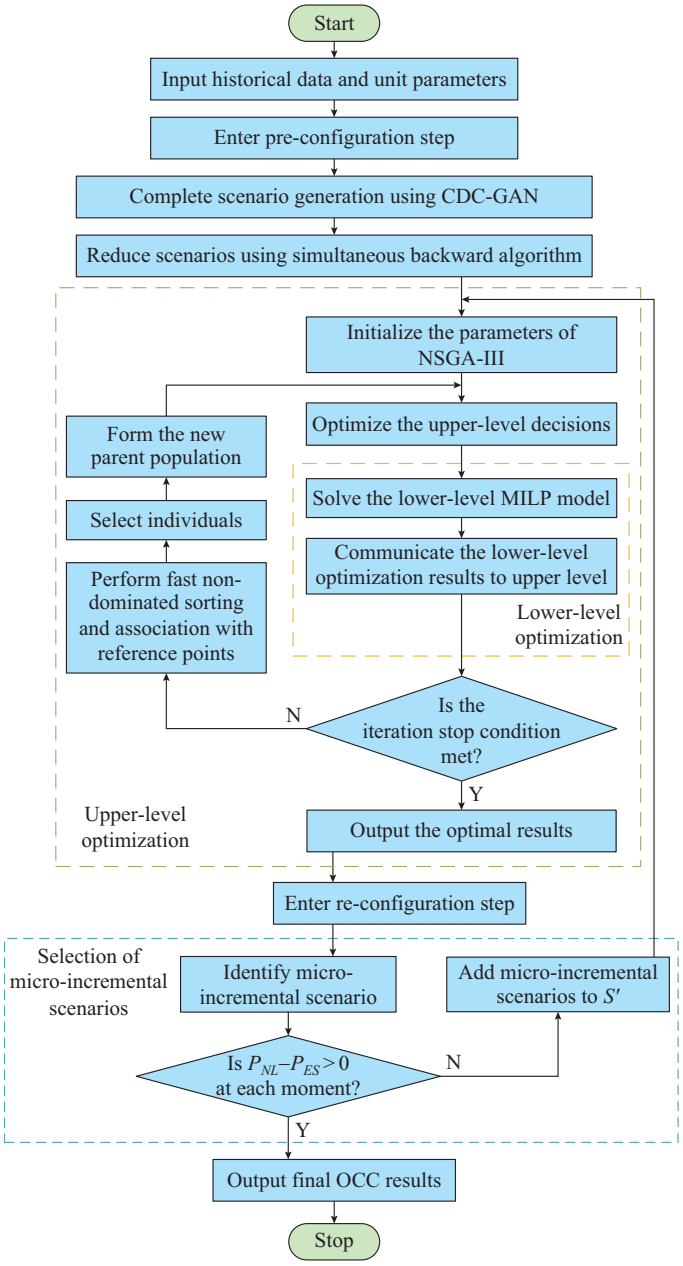

Fig. 1. Flowchart of multi-step optimization of large-scale energy base.

While the fundamental bi-level optimization structure employed under re-configuration shares similarities with that under pre-configuration, its key distinction lies in the incorporation of these micro-incremental scenarios. By feeding these scenarios into the optimization process, the re-configuration step allows for agile adjustments to the optimal results, in order to maintain supply and demand balance and prevent potential imbalances. Overall, by jointly using the multi-step optimization strategy with nested optimization structure, the OCC approach for the large-scale energy base is formed.

IV. Pre-configuration in Regular Scenarios

A. Stochastic Scenario Generation and Reduction

The input scenario vector $\boldsymbol{I}_{SV}$, which is composed of a time series of wind speed V_{WS}, solar irradiance R_{PV}, electric power load P_L, and H_L, is constructed as:

$$\boldsymbol{I}_{SV}=\left[V_{WS},R_{PV},P_L,H_L\right] \tag{19}$$

1) Complete Scenario Generation Using CDC-GAN

This part focuses on generating a large-scale number of combined wind, PV, electric power, and thermal power scenarios that conform to the original data distribution while taking into account the supply and demand relationships on both the source and load sides, which provides a reliable data basis for multi-scenario collaborative OCC.

The larger spatio-temporal scales of the large-scale energy base significantly increase the uncertainties on both source and load sides, which is a challenge to reflecting the strong coupling between electric, thermal, and hydrogen energy systems, particularly when seasonal variations exacerbate the inherent volatility of wind and PV power generation.

In this study, the CDC-GAN [31] is chosen for scenario generation. The goal is to enhance the precision of the generated samples by means of a mutual game played by the generator and the discriminator. Figure 2 shows the principle of the CDC-GAN.

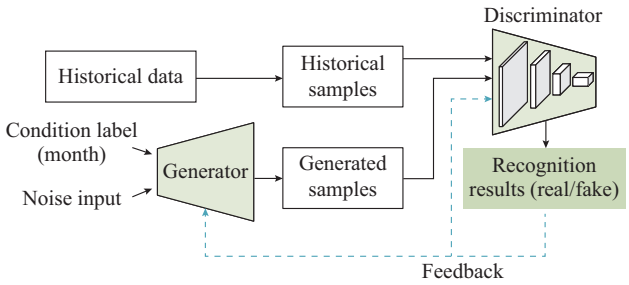

Fig. 2. Principle of CDC-GAN.

During the process of scenario generation on the source and load sides, the input dataset is categorized into four seasonal segments of spring, summer, autumn, and winter based on monthly divisions.

CDC-GAN captures seasonal characteristics of input data, while the joint generation of source-side and load-side scenarios reduces the computational burden integrating separate source and load scenario.

The generator contains two deconvolution layers to treat the input noise, and the discriminator contains two convolution layers to treat $\boldsymbol{I}_{SV}$. During the training phase [32], parameters of the discriminator and the generator are updated alternately and the condition label (month) of each scenario is trained simultaneously.

When the discriminator has an approximate output value for the true sample and the generated sample of the generator, the generator has captured the spatio-temporal and distribution characteristics of $\boldsymbol{I}_{SV}$.

2) Scenario Reduction Using Simultaneous Backward Algorithm

Selecting regular scenarios from a large number of scenarios requires scenario reduction. The jointly generated scenarios for each season are reduced using the simultaneous backward algorithm.

Step 1: suppose that there are N scenarios in set S. The

probability of each generated scenario is initialized as equal value, which means $P_s = 1/N$.

Step 2: calculate the probability distance between any two scenarios in the set S.

Step 3: find the nearest scenario S_m for each scenario S_i, based on the probability distances.

Step 4: remove the scenario S_m with the smallest probability distance from set S and update the scenario probability.

Step 5: the number of scenarios in set S is reduced to $N-1$. Repeat until the number of scenarios meets the requirements.

B. Pre-configuration Step

The pre-configuration step focuses on configuring the capacity of each unit based on regular scenarios.

The objective function of upper-level can be expressed as:

$$\min F_{Upper} = \begin{cases} F_1 = \sum_{i \in \Omega} C_{inv} + \mathbb{E}_p\left[F^*_{lower}\right] \\ F_2 = \sum_{s \in S} f_{mv,s} \\ F_3 = \sum_{s \in S} f_{ce,s} \end{cases} \tag{20}$$

where C_{inv} is the annualized investment cost; $\mathbb{E}_p\left[F^*_{lower}\right]$ is the expected annual operation cost, and in the pre-configuration step, the micro-incremental scenarios have not been selected; and $f_{mv,s}$ and $f_{ce,s}$ are the mean variances of load and carbon emission in scenario s, respectively.

Constraints of upper-level optimization are the pre-defined numerical ranges of each decision variable. The objective function at the lower-level optimization includes the operation costs in various scenarios, which can be described as:

$$\min F_{lower} = \sum_{i \in \Omega} \sum_{t=1}^{T} \left(\sum_{s \in S} \pi_s c_{i,ope} P_i(t,s) \right) \tag{21}$$

V. Re-configuration by Introducing Micro-incremental Scenarios

A. Selection of Micro-incremental Scenario

In practice, regular scenarios often fail to align precisely with the intricate and dynamic conditions, which may lead to supply and demand imbalances when being implemented using the OCC result in the regular scenarios. Thus, the selection of micro-incremental scenarios is studied in this subsection to compensate the set of regular scenarios.

Since the demand and supply of thermal power do not fluctuate in response to the stochastic variability of external factors such as wind and solar conditions, the supply and demand balance of thermal power is not considered. Under normal operation conditions, thermal power demands are consistently satisfied without requiring explicit accounting. Thus, this study prioritizes the assessment of supply and demand balance for electric power load, as thermal power load variations are relatively stable.

To address this limitation, this study proposes a compensation way. Initially, the supply and demand energy profiles are computed for all regular scenarios, leveraging the determined capacities from the pre-configuration step.

Then, a set of specialized micro-incremental scenarios is selected by focusing on identifying those moments of supply and demand imbalance. These micro-incremental scenarios are merged into the set of regular scenarios for the re-configuration step, enhancing the flexibility and efficiency of the final OCC.

Specifically, the net load P_{NL} and the maximum adjustable supply P_{ES} are two core metrics for evaluating the energy supply and demand balance, which are computed through (22) and (23), respectively.

$$P_{NL} = P_L - P_{PV} - P_{WT} \tag{22}$$

$$P_{ES} = P_{TP} + P_{CHP} + P_{grid} + P_{HCSS} + P_{VRB} - P_{EB} \tag{23}$$

s.t.

$$P_{ES}(t) < P_{NL}(t) \quad \exists t \in \{1, 2, \ldots, T\} \tag{24}$$

With the assistance of the CDC-GAN generated scenarios outlined in Section IV, scenarios that do not satisfy (24) are identified as micro-incremental scenarios. These scenarios serve to complement the operation characteristics not addressed by the regular scenarios. As shown in Supplementary Material A Fig. SA2, when the net load exceeds the maximum adjustable power supply, a potential risk of insufficient power supply is revealed.

B. Re-configuration Step

The re-configuration step involves merging the selected micro-incremental scenarios from Section V-A with the regular scenarios to create a more comprehensive set of scenarios. On this basis, the scenarios will undergo further optimization for configuration purposes.

Objective functions at upper level can be expressed as:

$$\min F_{Upper} = \begin{cases} F_1 = \sum_{i \in \Omega} C_{inv} + \mathbb{E}_p\left[F^*_{lower}\right] \\ F_2 = \sum_{s \in S \cup S'} f_{mv,s} \\ F_3 = \sum_{s \in S \cup S'} f_{ce,s} \end{cases} \tag{25}$$

Constraints of upper-level optimization are the pre-defined numerical ranges of each capacity decision variable.

Objective functions at lower level contain multiple scenarios for stochastic planning, which can be described as:

$$\min F_{lower} = \sum_{i \in \Omega} \sum_{t=1}^{T} \left(\sum_{s \in S} \pi_s c_{i,ope} P_i(t,s) + \sum_{s \in S'} \pi_s x(t,s) \kappa \right) \tag{26}$$

$$x(t,s) = \begin{cases} 0 & P_{ES}(t,s) \geq P_{NL}(t,s) \\ P_{ES}(t,s) - P_{NL}(t,s) & P_{ES}(t,s) < P_{NL}(t,s) \end{cases} \tag{27}$$

where κ is the coefficient penalizing the amount of load shedding in the objective function in micro-incremental scenarios.

VI. Validation and Analysis

The implemented approach, based on the nested use of

NSGA-III and YALMIP, is carried out using MATLAB to address the design problem of the large-scale energy base. The simulations were performed on a computer with an Intel Core i5-8250U processor (1.6 GHz) and 8 GB of RAM, running the Windows 10 operation system.

The computational performance of the proposed OCC approach varies depending on various scenarios. Generating the complete scenario set via CDC-GAN takes 24 min for 1000 scenarios. Reducing regular scenarios requires 2 min, yielding 12 scenarios. Pre-configuration takes 107.2 hours for 12 scenarios. Selecting micro-incremental scenarios requires 0.5 min, yielding 16 scenarios. Re-configuration takes 643.3 hours for 28 scenarios.

A. Pre-configuration Results Based on Regular Scenarios

Ten-year measured data are utilized from a large-scale energy base in Northwest China with a temporal resolution of one hour. Simple preprocessing of the data is performed: isolated forest for anomaly detection, linear interpolation for missing data, one-hour sliding window for average filtering, and min-max scaling for data normalization.

To ensure a sufficient quantity of reliable scenario data, the improved CDC-GAN generates 1000 scenarios, which are then categorized into the four seasons: spring, summer, autumn, and winter, based on the metadata labels embedded during the scenario generation. The cumulative distribution functions (CDFs) are obtained from distribution statistics for stochastic variables from original and generated scenarios, and the comparison is shown in Fig. 3, which are basically consistent. The CDF indicates that the scenario data generated by the improved CDC-GAN have the same data characteristics in original scenarios, which provides the data basis for the subsequent implementation of OCC.

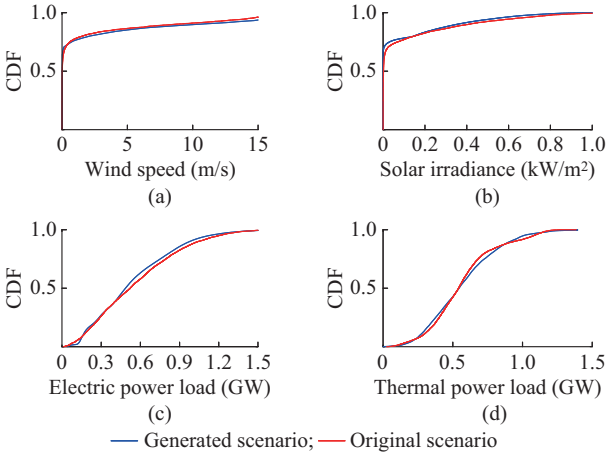

Fig. 3. Comparison of CDF for stochastic variables from original and generated scenarios. (a) Wind speed. (b) Solar irradiance. (c) Electric power load. (d) Thermal power load.

Generated scenarios with various season labels are reduced by the simultaneous backward algorithm. Figure 4 presents these stochastic variables in seasonal regular scenarios, which are normalized to per-unit values for ease of comparison. Each subplot depicts the normalized electric power load, solar irradiance, wind speed, and thermal power load. The maximum values for each variable are provided in the legend to indicate their actual scale. Supplementary Material A Table SAI presents an overview of the OCC results under regular scenarios. The multi-objective Pareto front solution set under pre-configuration is shown in Fig. 5, where TOPSIS is short for technique for order preference by similarity to ideal solution.

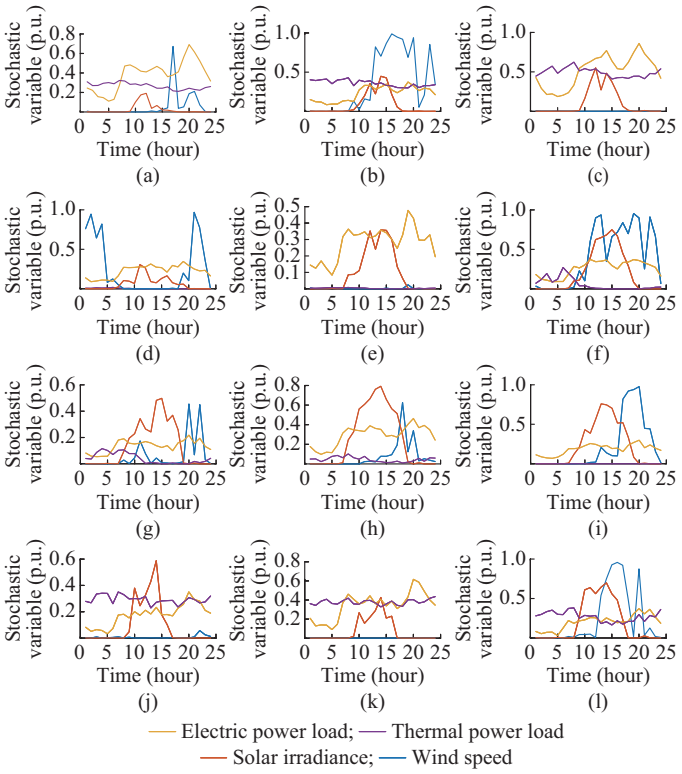

Fig. 4. Stochastic variables in seasonal regular scenarios. (a) Spring scenario 1. (b) Spring scenario 2. (c) Spring scenario 3. (d) Summer scenario 1. (e) Summer scenario 2. (f) Summer scenario 3. (g) Autumn scenario 1. (h) Autumn scenario 2. (i) Autumn scenario 3. (j) Winter scenario 1. (k) Winter scenario 2. (l) Winter scenario 3.

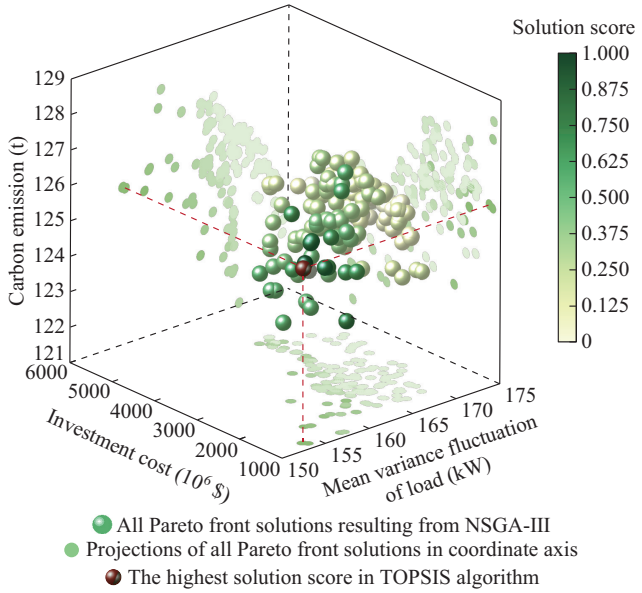

Fig. 5. Multi-objective Pareto front solution set under pre-configuration.

B. Re-configuration Results Based on Merged Scenarios

The results and optimization metrics are described and analyzed in this subsection. The capacity of each unit is configured for regular scenarios in the pre-configuration step. To ensure that the configuration results remain highly robust in a multivariate environment, 16 micro-incremental scenarios are selected in this study. One of these scenarios is shown in Fig. 6. The probability of each scenario is set to be 0.001.

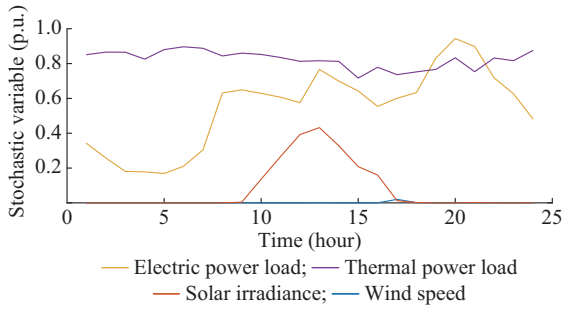

Fig. 6. One of 16 micro-incremental scenarios for stochastic variables.

The results before re-configuration, as shown in Fig. 7(a), show that the supply and demand balance in these scenarios cannot be satisfied, and power supply gaps usually exist at certain moments during the peak power consumption or rapid increase in electric power load.

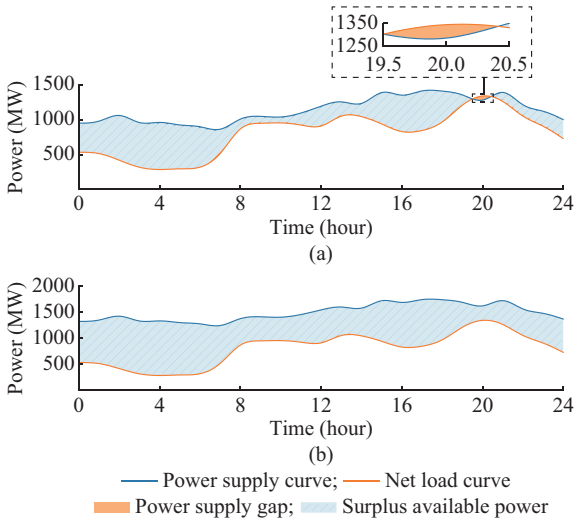

Fig. 7. Comparison of supply and demand balance before and after re-configuration. (a) Before re-configuration. (b) After re-configuration.

Re-configuration corrects the pre-configured results. In this process, the nested optimization structure uses multiple optimization objectives (F_1, F_2, F_3) at the upper level. At the lower level, regular scenarios, micro-incremental scenarios, and new scenario probabilities are combined to form a new objective function.

The multi-objective Pareto front solution set under re-configuration is shown in Fig. 8. The set has a regular trend between each two metrics on the projection surface of the coordinate axis, but the three metrics show complex characteristics in three-dimensional space, which indicates that it is almost impossible to obtain the best solution among economy, output fluctuation, and carbon emission at the same time.

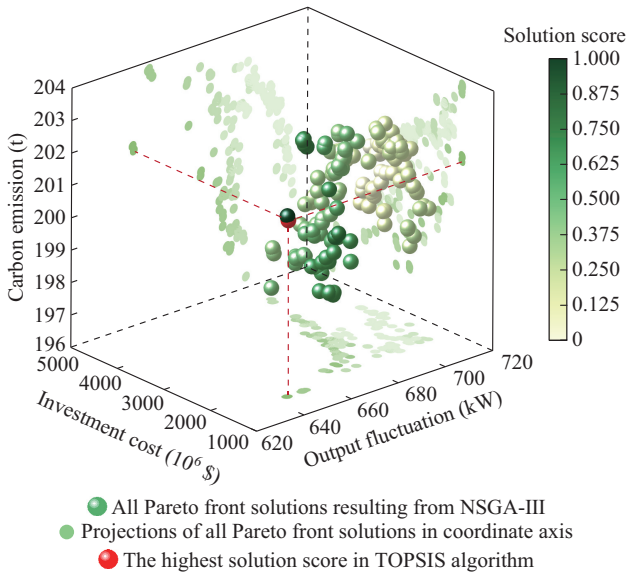

Fig. 8. Multi-objective Pareto front solution set under re-configuration.

Therefore, it is necessary to compromise the optimization metrics according to the actual demands in all OCC processes. We select a suitable solution through TOPSIS algorithm.

Table I shows the supply and demand balance of the 16 micro-incremental scenarios before and after re-configuration by calculating the minimum difference between P_{NL} and P_{ES}, which indicates that there is an under-supplied moment in the scenario if the minimum value of $P_{NL}-P_{ES}$, i.e., $\{P_{NL}-P_{ES}\}_{\min}$, is less than 0. It can be observed that all the power shortage situations of the micro-incremental scenarios are improved after re-configuration.

TABLE I
SUPPLY AND DEMAND BALANCE FOR 16 MICRO-INCREMENTAL SCENARIOS BEFORE AND AFTER RE-CONFIGURATION

Scenario number	$\{P_{NL}-P_{ES}\}_{\min}$ under pre-configuration (MW)	$\{P_{NL}-P_{ES}\}_{\min}$ under re-configuration (MW)
1	−176	170
2	−284	77
3	−106	238
4	−287	74
5	−17	317
6	−339	38
7	−293	64
8	−347	20
9	−336	30
10	−300	56
11	−326	40
12	−64	272
13	−340	27
14	−350	17
15	−186	176
16	−147	196

Compared with the results of pre-configuration, the supply and demand imbalance is completely eliminated, regarded as the highest priority, as shown in Fig. 8, while the OCC metrics of the large-scale energy base have different degrees of deterioration within the acceptable range, as shown in Table II, indicating that although the probability of micro-incremental scenarios is small, its impact on the OCC result is significant.

TABLE II
CONFIGURATION RESULTS AND METRICS

Decision variable	After pre-configuration	After re-configuration
Installation area of PV panel	156000 (m^2)	357000 (m^2)
Wind turbine capacity	103 (MW)	137 (MW)
Energy storage capacity of VRB	36 (MWh)	60 (MWh)
Volume of hydrogen storage unit	159000 ($N \cdot m^3$)	279000 ($N \cdot m^3$)
Rated power of CHP unit	1351 (MW)	1219 (MW)
Rated power of thermal power unit	313 (MW)	369 (MW)
Energy storage capacity of electric-heating molten salt boiler	329 (MW)	337 (MW)
Energy storage capacity of heat storage tank	187 (MWh)	210 (MWh)
F_1	1.27×10^{10} ($)	1.69×10^{10} ($)
F_2	153 (kW)	646 (kW)
F_3	1.26×10^4 (kg)	2.01×10^5 (kg)

To satisfy more stringent balance requirements between supply and demand, the re-configuration results in a significant increase in total capacity. The proportion of fossil fuel generation capacity decreases from 86.5% to 76.2%, while the proportion of renewable energy generation capacity increases from 13.5% to 23.8%. This change reflects a transition in the energy supply structure of the electric power system from a relatively high-carbon emitting system to a low-carbon system.

In Fig. 7(b), the net load and power supply after re-configuration are presented, which consider micro-incremental scenarios. After re-configuration, micro-incremental scenarios achieve the balance between supply and demand. Therefore, the proposed OCC approach greatly improves the reliability of energy supply.

To analyze the outcomes of hourly electric and thermal power co-dispatch, regular autumn scenario 1 is utilized as the operational context, which is characterized by significant availability of both wind and solar resources, alongside pronounced peaks in both electric and thermal power demands.

Figure 9 shows the output of units under pre-configuration and re-configuration in regular autumn scenario 1. The upper portion of each bar indicates the hourly energy output of the units, the lower portion indicates the hourly energy storage of the units.

The load in the early morning is low. Therefore, the majority of the electric power is supplied by the grid P_{grid} to satisfy customer demands. From the 0^{th} hour to 11^{th} hour, P_{EB} consumes electric power to generate thermal power, which constitutes most of H_{EB} during this period.

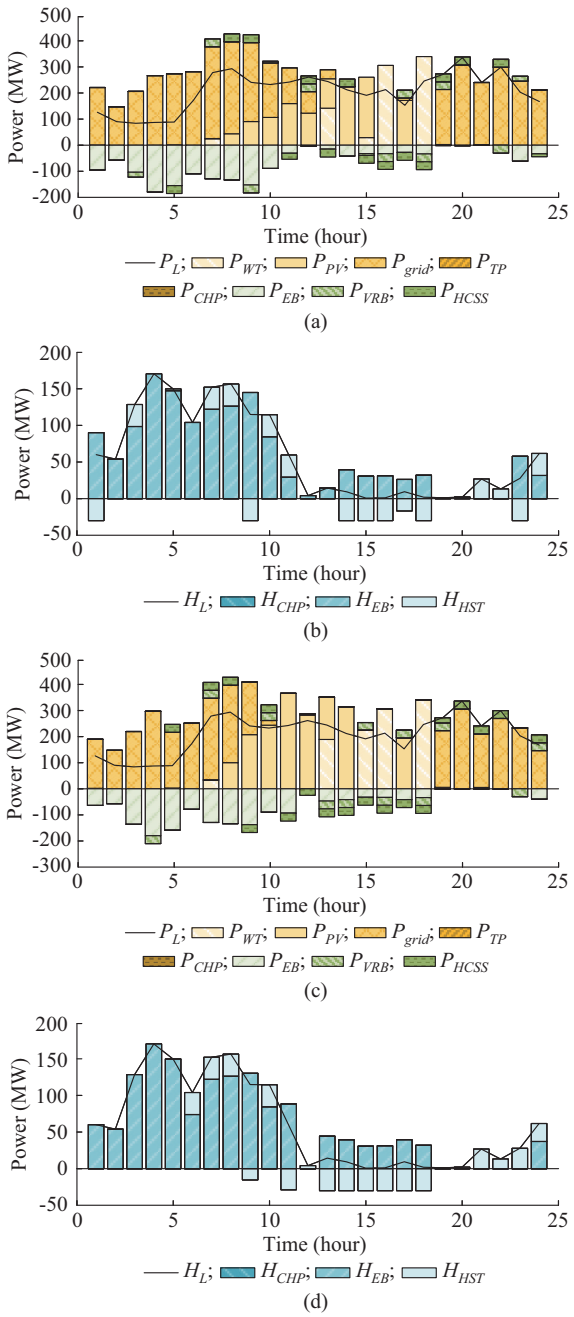

Fig. 9. Output of units under pre-configuration and re-configuration in regular autumn scenario 1. (a) Electric power output and storage of units under pre-configuration. (b) Thermal power output and storage of units under pre-configuration. (c) Electric power output and storage of units under re-configuration. (d) Thermal power output and storage of units under re-configuration.

During the peak period of electric power consumption, the thermal storage unit releases stored thermal power, thereby reducing the demand for electric power that would be needed for heating.

To meet the load demand in the morning, in addition to purchasing electric power from the grid, the electric power is supplied by storage units, including VRB discharging power and electric-hydrogen conversion units. During low load periods, excess electric power P_{VRB} is stored in VRBs.

As solar radiation increases, PV power begins to contrib-

ute significantly at the 8th hour. Wind power provides more power in the afternoon. P_{WT} and P_{PV} gradually increase to become the primary daytime power supply, respectively. Any surplus energy is then stored: electric power is directed to VRBs for charging, thermal power is accumulated in heat storage tank, and hydrogen is produced and stored by hydrogen storage unit. Thermal supply in the evening is mainly provided by the electric-heating molten salt boiler.

A primary outcome of the re-configuration, particularly evident on this regular day, is the enhanced contribution from wind and PV power, stemming from their increased installed capacities. During the 9th hour and 18th hour, wind and PV power can cover almost all the electric power and thermal power demands, which greatly reduces the grid pressure during the daytime and enhances grid flexibility. At the same time, more energy conversion and storage units enhance the supply reliability during sudden electric and thermal power demand fluctuations.

Figures 10 and 11 illustrate the storage and release of VRB, thermal, and hydrogen at various moments in regular autumn scenario 1. They show the hourly energy output for charging/discharging and energy storage levels over time. The broken lines represent the energy in storage units.

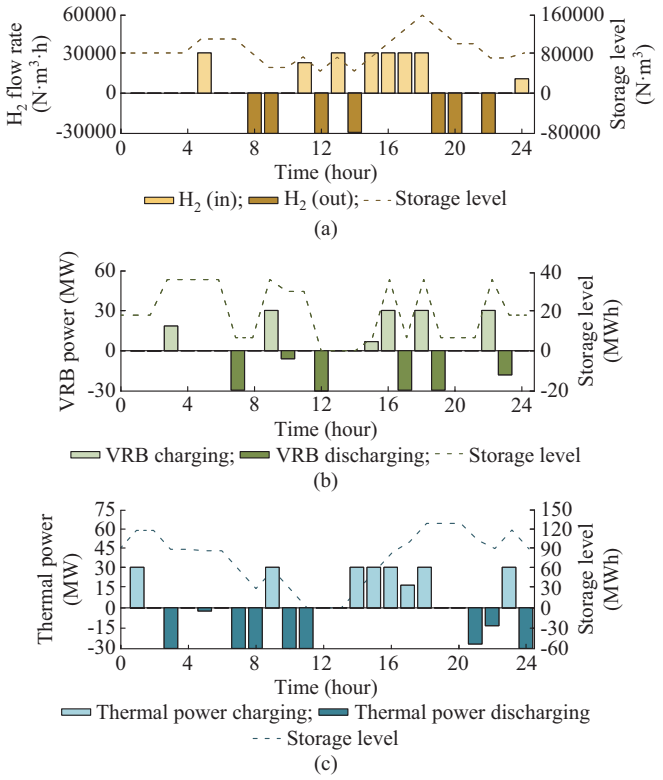

Fig. 10. Storage and release of energy storage units under pre-configuration in regular autumn scenario 1. (a) H_2 flow rate and storage level under pre-configuration. (b) VRB power and storage level under pre-configuration. (c) Thermal power and storage level under pre-configuration.

The inclusion of micro-incremental scenarios leads to an increased capacity of the energy storage units compared with the pre-configuration without such considerations. Consequently, these re-configuration units can provide more electric and thermal power during peak evening hours. Furthermore, during daytime periods with high wind and PV power generation, the increased storage capacity allows for greater accumulation of energy, resulting in higher storage levels of electric power, thermal power, and hydrogen.

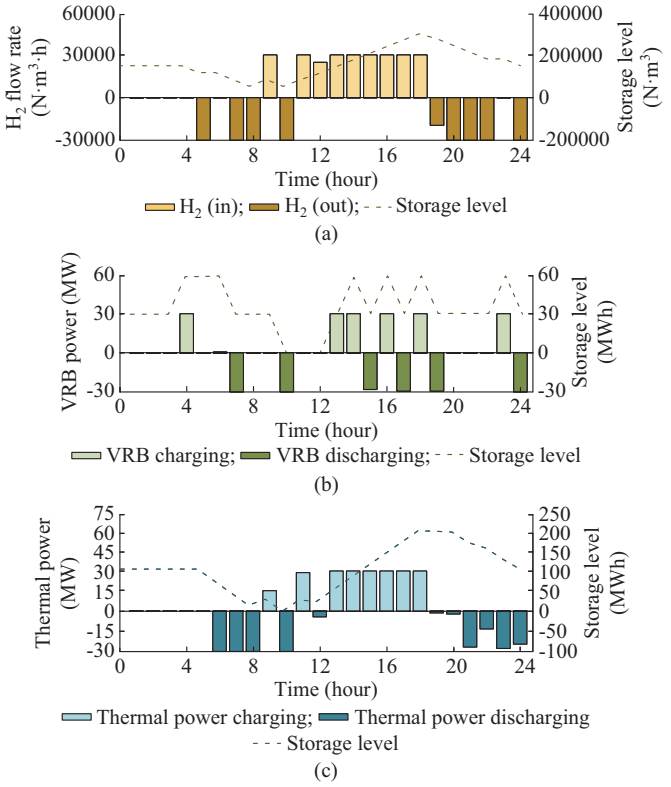

Fig. 11. Storage and release of energy storage units under re-configuration in regular autumn scenario 1. (a) H_2 flow rate and storage level under re-configuration. (b) VRB power and storage level under re-configuration. (c) Thermal power and storage level under re-configuration.

VII. Conclusion

The operation of a large-scale energy base is affected by both external disturbances and interactive operation characteristics. The coupling of stochastic sources and loads further complicates the OCC of various units. We introduce the system theory to obtain the nonlinear state-space description for systematic analysis of external stochastic influence and internal interaction in the large-scale energy base. Considering interactive multi-timescale objectives between annual and daily ones, a nested optimization structure is established including upper-level and lower-level optimization using annual and daily cumulative objectives, respectively. A multi-dimensional optimization space is constructed considering economy, output fluctuation, and carbon emission while transforming the complex optimization problem into hierarchical ones, improving the solving efficiency and quality.

Furthermore, considering external multi-stochastic scenarios, a multi-step optimization strategy is proposed including pre-configuration in regular scenarios and re-configuration by introducing micro-incremental scenarios. This strategy utilizes the micro-incremental scenarios to compensate and correct the regular scenarios. The multi-step optimization strategy and nested optimization structure jointly achieve the

OCC of the large-scale energy base. In each step, the nested optimization structure is executed once.

Finally, through validation of case analysis, the imbalance between electric power supply and load demand are eliminated, highly enhancing the optimal configuration effect.

This study does not focus on developing a precise energy management system but prioritizes long-term capacity optimization, recognizing that rising renewable energy demand and increasing volatility of net load profiles driven by enhanced environmental awareness, and policy incentives will necessitate incorporating stochastic scenarios into the planning of energy infrastructure. Consequently, the proposed multi-step optimization strategy, featuring a nested optimization structure, is well-suited for the construction and OCC of large-scale, compositionally diverse energy bases, especially when addressing complex operational conditions.

REFERENCES

[1] Y. Wang, Y. Wang, Y. Huang *et al*., "Optimal scheduling of the regional integrated energy system considering economy and environment," *IEEE Transactions on Sustainable Energy*, vol. 10, no. 4, pp. 1939-1949, Oct. 2019.

[2] Y. Zhang, Q. Hua, L. Su *et al*., "Life cycle optimization of renewable energy systems configuration with hybrid battery/hydrogen storage: a comparative study," *Journal of Energy Storage*, vol. 30, p. 101470, Aug. 2020.

[3] M. Jahannoosh, S. A. Nowdeh, A. Naderipour *et al*., "New hybrid meta-heuristic algorithm for reliable and cost-effective designing of photovoltaic/wind/fuel cell energy system considering load interruption probability," *Journal of Cleaner Production*, vol. 278, p. 123406, Jan. 2021.

[4] M. J. H. Moghaddam, A. Kalam, S. A. Nowdeh *et al*., "Optimal sizing and energy management of stand-alone hybrid photovoltaic/wind system based on hydrogen storage considering LOEE and LOLE reliability indices using flower pollination algorithm," *Renewable Energy*, vol. 135, pp. 1412-1434, May 2019.

[5] W. Huang and N. Zhang, "Optimal configuration planning of multi-energy systems considering distributed renewable energy," *IEEE Transactions on Smart Grid*, vol. 10, no. 2, pp. 1452-1464, Mar. 2019.

[6] Y. Wang, N. Zhang, Z. Zhuo *et al*., "Mixed-integer linear programming-based optimal configuration planning for energy hub: starting from scratch," *Applied Energy*, vol. 210, pp. 1141-1150, Jan. 2018.

[7] H. Saber, M. Moeini-Aghtaie, M. Ehsan *et al*., "A scenario-based planning framework for energy storage systems with the main goal of mitigating wind curtailment issue," *International Journal of Electrical Power & Energy Systems*, vol. 104, pp. 414-422, Jan. 2019.

[8] C. Ma, S. Dong, and J. Lian, "Multi-objective sizing of hybrid energy storage system for large-scale photovoltaic power generation system," *Sustainability*, vol. 11, no. 19, p. 5441, Mar. 2019.

[9] C. Xu, Y. Ke, Y. Li *et al*., "Data-driven configuration optimization of an off-grid wind/PV/hydrogen system based on modified NSGA-II and CRITIC-TOPSIS," *Energy Conversion and Management*, vol. 215, p. 112892, Jul. 2020.

[10] J. Zhao, Z. Wu, H. Long *et al*., "Optimal operation control strategies for active distribution networks under multiple states: a systematic review," *Journal of Modern Power Systems and Clean Energy*, vol. 12, no. 5, pp. 1333-1344, Sept. 2024.

[11] X. Yang, Y. Xu, N. Yang *et al*., "Research on the reliability and capacity allocation of wind power-solar power-pumped storage hybrid power system," in *Proceedings of 2018 China International Conference on Electricity Distribution (CICED)*, Tianjin, China, Sept. 2018, pp. 2071-2076.

[12] C. Wang, W. Wei, Y. Xie *et al*., "Capacity sizing of the integrated wind-solar-storage system: a nested game approach," *IET Generation, Transmission & Distribution*, vol. 16, no. 14, pp. 2852-2863, Jan. 2022.

[13] M. Wang, M. Yang, Z. Fang *et al*., "A practical feeder planning model for urban distribution system," *IEEE Transactions on Power Systems*, vol. 38, no. 2, pp. 1297-1308, Apr. 2023.

[14] A. Kaabeche and Y. Bakelli, "Renewable hybrid system size optimization considering various electrochemical energy storage technologies," *Energy Conversion and Management*, vol. 193, pp. 162-175, Aug. 2019.

[15] Y. Zheng and S. Xie, "The optimal configuration planning of energy hubs in urban integrated energy system using a two-layered optimization method," *International Journal of Electrical Power & Energy Systems*, vol. 123, p. 106257, Jun. 2020.

[16] A. Afzal and M. K. Ramis, "Multi-objective optimization of thermal performance in battery system using genetic and particle swarm algorithm combined with fuzzy logics," *Journal of Energy Storage*, vol. 32, p. 101815, Dec. 2020.

[17] Y. Li, Y. Zou, Y. Tan *et al*., "Optimal stochastic operation of integrated low-carbon electric power, natural gas, and heat delivery system," *IEEE Transactions on Sustainable Energy*, vol. 9, no. 1, pp. 273-283, Jan. 2018.

[18] P. Li, Z. Wang, H. Liu *et al*., "Bi-level optimal configuration strategy of community integrated energy system with coordinated planning and operation," *Energy*, vol. 236, p. 121539, Jul. 2021.

[19] S. Lin, C. Liu, Y. Shen *et al*., "Stochastic planning of integrated energy system via Frank-Copula function and scenario reduction," *IEEE Transactions on Smart Grid*, vol. 13, no. 1, pp. 202-212, Nov. 2022.

[20] U. Akram, N. Mithulananthan, M. Q. Raza *et al*., "RoCoF restrictive planning framework and wind speed forecast informed operation strategy of energy storage system," *IEEE Transactions on Power Systems*, vol. 36, no. 1, pp. 224-234, Jan. 2021.

[21] S. Zeynali, N. Rostami, A. Ahmadian *et al*., "Two-stage stochastic home energy management strategy considering electric vehicle and battery energy storage system: an ANN-based scenario generation methodology," *Sustainable Energy Technologies and Assessments*, vol. 39, p. 100722, Jun. 2020.

[22] Y. Li, J. Li, and Y. Wang, "Privacy-preserving spatiotemporal scenario generation of renewable energies: a federated deep generative learning approach," *IEEE Transactions on Industrial Informatics*, vol. 18, no. 4, pp. 2310-2320, Apr. 2022.

[23] Y. Chen, Y. Wang, D. Kirschen *et al*., "Model-free renewable scenario generation using generative adversarial networks," *IEEE Transactions on Power Systems*, vol. 33, no. 3, pp. 3265-3275, May 2018.

[24] Z. Geng, C. Shi, and Y. Han, "Intelligent small sample defect detection of water walls in power plants using novel deep learning integrating deep convolutional GAN," *IEEE Transactions on Industrial Informatics,* vol. 19, no. 6, pp. 7489-7497, Mar. 2023.

[25] Z. Li, W. Li, S. Y. Samson *et al*., "Fast frequency response reserve planning for power systems considering homogeneous extreme risks," *IEEE Transactions on Industry Applications*, vol. 59, no. 2, pp. 2314-2325, Mar. 2023.

[26] Y. Wu, J. Wang, Y. Song *et al*., "Resilience-oriented valuation for energy storage amidst extreme events," *Electrical Engineering*, vol. 9, no. 3, pp. 15-25, Sept. 2023.

[27] X. Wang and Z. Bie, "Bi-level planning for integrated electricity and natural gas systems with wind power and natural gas storage," *International Journal of Electrical Power & Energy Systems*, vol. 118, p. 105738, Jun. 2020.

[28] G. Mavromatidis, K. Orehounig, and J. Carmeliet, "Design of distributed energy systems under uncertainty: a two-stage stochastic programming approach," *Applied Energy*, vol. 222, pp. 932-950, Jul. 2018.

[29] Y. Zhang, Z. Lu, D. Ma *et al*., "Ripple-GAN: lane line detection with ripple lane line detection network and Wasserstein GAN," *IEEE Transactions on Intelligent Transportation Systems*, vol. 22, no. 3, pp. 1532-1542, Mar. 2020.

[30] K. Deb and H. Jain, "An evolutionary many-objective optimization algorithm using reference-point-based nondominated sorting approach, part I: Solving problems with box constraints," *IEEE Transactions on Evolutionary Computation*, vol. 18, no. 4, pp. 577-601, Aug. 2014.

[31] Y Chen, Y Wang, D Kirschen *et al*., "Model-free renewable scenario generation using generative adversarial networks," *IEEE Transactions on Power Systems*, vol. 33, no. 3, pp. 3265-3275, Feb. 2018.

[32] B. Lin and J. Ge, "Does institutional freedom matter for global forest carbon sinks in the face of economic development disparity?" *China Economic Review*, vol. 65, p. 101563, Feb. 2021.

Yini Wang received the B.E. degree from Anhui University of Science and Technology, Huainan, China, in 2022. She is currently working toward the M.E. degree in North China Electric Power University, Beijing, China. Her research interests include optimal capacity configuration and dispatch of integrated energy system.

Yang Hu received the Ph.D. degree in thermal power engineering from the

School of Energy, Power, and Mechanical Engineering, North China Electric Power University, Beijing, China, in 2015. He is currently with the School of Control and Computer Engineering, North China Electric Power University. His research interests include control and data analysis of renewable-energy power system, virtual power plant, microgrid, and integrated energy system.

Yueli Zhao received the B.E. degree from North China Electric Power University, Baoding, China, in 2021. She is currently working toward the M.E. degree in control engineering. Her research interests include optimal capacity configuration of integrated energy system.

Yunzhi Li received the B. E. degree of engineering major in automation from the School of Control and Computer Engineering, North China Electric Power University, Beijing, China, in 2016. He is currently working toward the Ph. D. degree in control theory and control engineering. His research interests include power system operation and economy, demand-side management, and integrated energy system.

Fang Fang received the Ph. D. degree in thermal power engineering from North China Electric Power University, Beijing, China, in 2005. He is currently a Professor with the School of Control and Computer Engineering, North China Electric Power University. His current research interests include optimal configuration and operation of integrated energy system, Internet of Things technologies in modern power system, and intelligent power generation technology.

Jizhen Liu received the M.S. degree in power engineering from North China Institute of Electric Power, Beijing, China, in 1982. He is currently a Member of the Chinese Academy of Engineering and a Professor with the State Key Laboratory of Alternate Electrical Power System with Renewable Energy Sources, North China Electric Power University, Beijing, China. His research interests include renewable-energy power system and intelligent power generation theory and technology.